

The Asymmetric Boundary Layer Flow Under a Translating Hurricane

LLOYD J. SHAPIRO

Hurricane Research Division, AOML/NOAA, Miami, FL 33149

(Manuscript received 22 October 1982, in final form 7 April 1983)

ABSTRACT

An investigation is made of the role of the translation of a hurricane in determining the distribution of boundary layer winds and in the organization of convection. A slab boundary layer model of constant depth is used to analyze the steady flow under a specified translating symmetric vortex in gradient balance. A truncated spectral formulation is used, including asymmetries through wavenumber 2. The role of linear and nonlinear asymmetric effects in the determination of the boundary layer response is diagnosed. These effects are relevant to relatively slowly and rapidly translating hurricanes, respectively.

The analysis is compared to observations of Hurricanes Frederic of 1979 and Allen of 1980, as well as to other observational and theoretical studies. Allen's translation speed was approximately twice that of Frederic. It is found that the simple boundary layer formulation simulates the qualitative features of the wind field observed in Frederic. The distribution of convection in Frederic and Allen compares favorably with boundary layer convergence diagnosed from the model.

1. Introduction

The structure and evolution of a hurricane are controlled by a complex interaction between convective, mesoscale and synoptic-scale processes. Convergence of moisture in the planetary boundary layer is a primary mechanism for organization of the convection in the inner core of an intense hurricane (Ooyama, 1982). The convection, in turn, provides the diabatic heating necessary to sustain the hurricane. The distribution of winds in the boundary layer also determines much of the hurricane's destructive potential.

A translating symmetric hurricane vortex will have stronger winds relative to the earth on the right side of the direction of motion, simply due to the addition of the translation velocity to the storm circulation. The asymmetric winds are accompanied by an asymmetry in boundary layer frictional drag. The asymmetry in drag forces an asymmetry in boundary layer winds and convergence, and thus in the hurricane's distribution of convection.

This paper investigates the role of the translation of a hurricane in determination of the distribution of boundary layer winds and in the organization of the convection. A simple slab boundary layer model is used to analyze the steady boundary layer flow under a translating symmetric hurricane vortex. The feedback of the induced asymmetric convective distribution to the structure of the hurricane is not included. The results of the analysis are compared to observational studies of moving hurricanes.

Previous observational and theoretical studies are discussed in the next section. Section 3 presents the physical model, with an evaluation of the symmetric

boundary layer flow under a stationary hurricane. The formulation of a truncated spectral representation in Section 4 is followed by an evaluation of the asymmetric flow under a moving hurricane in Section 5. Section 6 presents a simplified quasi-linear version of the analysis, valid for a slowly moving hurricane. The role of linear and nonlinear asymmetric effects in determining the wind and convergence distribution is diagnosed in Section 7. Section 8 presents a further discussion of the results.

2. Previous Studies

a. Observations

Recent analyses of the boundary layer winds in Hurricane Frederic of 1979 (Powell, 1982) have highlighted the relationship between the distribution of winds and convection and the motion of the hurricane. Fig. 1 (Mark Powell, personal communication, 1982) shows the observed isotach distribution in the boundary layer of Frederic while it was over open water in the Gulf of Mexico. The data and compositing technique used in deriving the winds are described in Powell (1982). In Fig. 1 the winds are expressed in a coordinate system that translates with the hurricane at $\sim 5 \text{ m s}^{-1}$ toward the NNW, as indicated by the arrow. This translation speed is about the average for all hurricanes. In the translating system the winds are stronger to the left of the direction of motion than to the right. Powell (1982, his Fig. 9) found stronger winds to the right, relative to the earth. In either case the isotach maximum is ahead of the storm, with maximum winds 45 m s^{-1} roughly 30 km

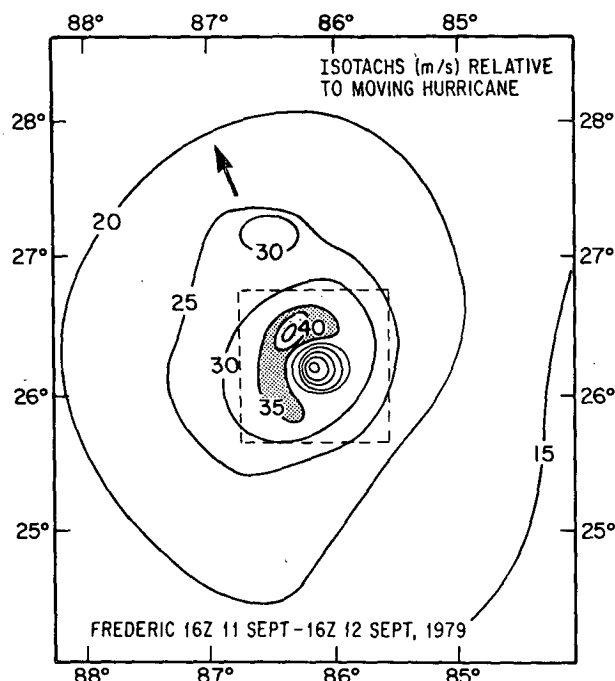


FIG. 1. Isotachs of Hurricane Frederic composite relative to translating hurricane. Dashed line delineates approximate area covered by Fig. 2. Courtesy of Mark Powell.

in front of the center of the circulation. Hughes (1952) found maximum winds relative to the ground in the right-rear quadrant of other hurricanes. It is difficult to relate his results to the present study, however, since he used a much coarser analysis.

The highly asymmetric wind field in Frederic is associated with an asymmetric convective distribution, as illustrated by the radar presentation in Fig. 2. This figure, prepared by Dave Jorgensen and Frank Marks (personal communication, 1982), is a time composite derived from individual radar sweeps at the 1.5 km level over an interval near the middle of that covered by the wind composite in Fig. 1. The dashed line in Fig. 1 delineates the approximate area covered by Fig. 2. The relationship between boundary layer convergence, convection and radar reflectivity is not directly one-to-one. Nevertheless, the broad arc of high reflectivity [>40 dB(Z)] in Fig. 2 does imply enhanced boundary layer convergence oriented ahead of the storm. This broken eyewall is nearly coincident with the isotach maximum in Fig. 1. The convection surrounds a nearly circular clear eye. A very similar pattern of reflectivity was observed in Hurricane David of 1979 (see Fig. 5, Willoughby *et al.*, 1982) and in Hurricane Floyd of 1981 (Dave Jorgensen, personal communication, 1982), which were also translating at ~ 5 m s $^{-1}$. Frederic, during other time intervals, had reflectivity patterns implying convergence concentrated more in the right front quadrant (cf. Fig. 8 of Powell, 1982). Hughes (1952) found

maximum inflow in the right front quadrant. Powell (1982) found maximum inflow angles in the right rear quadrant, but did not evaluate the radial wind.

Fig. 3 shows a radar composite of Hurricane Allen on 7 August 1980. At that time the hurricane's surface pressure was in a quasi-steady state, just following a contraction phase in a concentric eye cycle (Willoughby *et al.*, 1982). A similar, but less distinct, distribution of radar reflectivity was evident on 8 August (Fig. 13 of Willoughby *et al.*, 1982). The hurricane was translating to the west, in the direction of the arrow, at ~ 9 m s $^{-1}$; the radius of maximum wind (RMW) was ~ 20 km. The translation speed is about twice that of Frederic. As in Frederic (Fig. 2), the convection is concentrated ahead of the storm. There is a secondary convective feature [35 dB(Z)] in the left rear quadrant, and an indication of enhanced convection [30 dB(Z)] in the right front. The clear eye has an elliptical outline, with the major axis oriented almost normal to the direction of motion.

b. Theoretical studies

The steady asymmetric boundary layer under a moving hurricane has been studied theoretically by Myers and Malkin (1961) and Chow (1971). Myers and Malkin (1961) made a Lagrangian parcel trajectory analysis to deduce the flow under a hurricane vortex with a specified symmetric pressure distribution. They implicitly assumed that the hurricane translated in the absence of a large-scale steering flow. An empirically determined frictional drag was used,

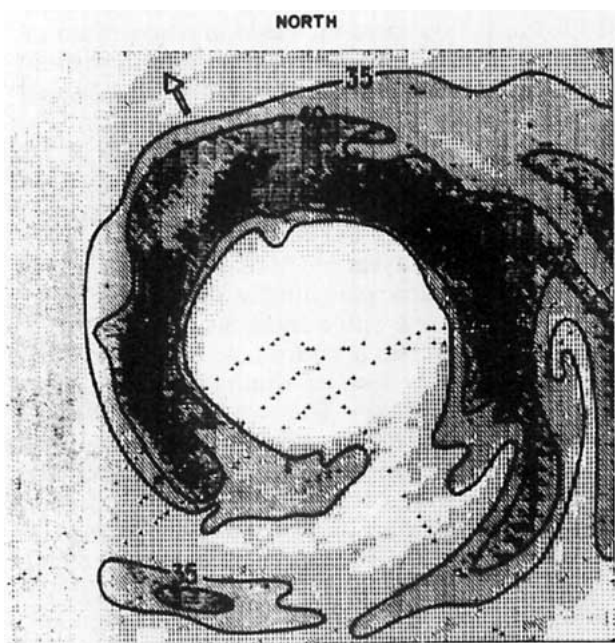


FIG. 2. Hurricane Frederic radar composite from 0135 GMT to 0336 GMT on 12 September 1979. Contours are in dB(Z). Domain is 120 km \times 120 km. Courtesy of Dave Jorgensen and Frank Marks.

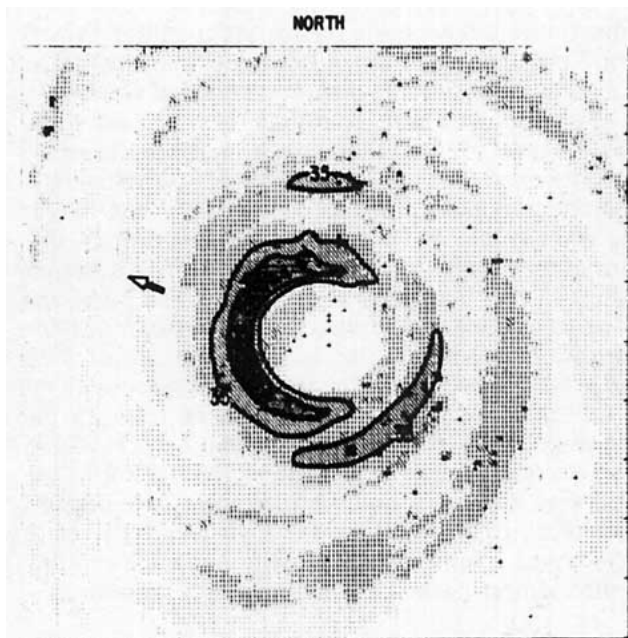


FIG. 3. As in Fig. 2, but for Hurricane Allen from 1705 GMT to 2135 GMT on 7 August 1980.

with nearly equal tangential and normal components proportional to the square of the wind speed. Myers and Malkin found maximum convergence in the right front quadrant for a hurricane moving at $\sim 10 \text{ m s}^{-1}$. When the translation speed was increased from 5 to 10 m s^{-1} the isotach maximum (relative to the earth) rotated from in front of the storm to the right front. As the translation speed increased, the maximum inflow angle similarly rotated clockwise from in front to the right front; there was also an indication that the radius of maximum wind decreased.

Chow (1971), working under the direction of Vic Ooyama at New York University, made a numerical integration of the horizontal momentum equations in Cartesian coordinates translating with the hurricane vortex. As in Myers and Malkin's analysis, Chow specified a symmetric pressure distribution and a slab boundary layer, but with a frictional drag parallel to the (total) wind. The pressure field was in gradient balance in a vortex with maximum wind of 42.5 m s^{-1} at a radius of 40 km. The vortex translated at 10 m s^{-1} . Chow calculated the boundary layer wind and convergence for cases with and without a large-scale geostrophic steering current equal to the translation velocity. In the former case, winds were greater on the left than on the right, relative to a coordinate system that translated with the storm; relative to the earth, the winds were greater on the right than left. The isotach maximum was in front. Maximum inflow and convergence were in the right front quadrant. The isotach distribution was very similar to that of Hurricane Frederic.

The physical model used in the present study is very similar to that of Chow (1971). In the present model, however, a truncated spectral analysis in cylindrical coordinates is used to diagnose the boundary layer wind field. Although algebraically more involved, this method allows a simple separation and diagnosis of various effects and facilitates interpretation of the results. Particular attention is given to the positions of the maximum wind, inflow and convergence, and their dependence on the translation speed of the hurricane. The results will be related to the observations and theoretical analyses described above.

3. Physical model: Solution for stationary hurricane

As in Chow (1971), the momentum equations are solved for a slab boundary layer of constant depth under an imposed symmetric pressure distribution. The coordinate system translates with the hurricane vortex, which is in gradient balance with the pressure above the boundary layer. In cylindrical coordinates the radial and tangential momentum equations are

$$u \frac{\partial u}{\partial r} - \frac{v^2}{r} - fv + \frac{v}{r} \frac{\partial u}{\partial \lambda} + \frac{\partial \phi}{\partial r} - K \left(\nabla^2 u - \frac{u}{r^2} - \frac{2}{r^2} \frac{\partial v}{\partial \lambda} \right) + F(c, u) = 0, \quad (1a)$$

$$u \left(\frac{\partial v}{\partial r} + \frac{v}{r} \right) + fu + \frac{v}{r} \frac{\partial v}{\partial \lambda} - K \left(\nabla^2 v - \frac{v}{r^2} + \frac{2}{r^2} \frac{\partial u}{\partial \lambda} \right) + F(c, v) = 0. \quad (1b)$$

A list of symbols used in the text is given in Appendix A. The advective and diffusive terms in (1a) and (1b) are derived in Batchelor (1967, his Appendix 2). The hurricane vortex is translating with velocity c . In the present analysis the background geostrophic wind associated with a large-scale pressure gradient is assumed to equal the translation velocity. Then, c enters only through the frictional drag $F(c, u)$. Here (u, v) are the (radial, tangential) components of the velocity vector \mathbf{u} , relative to the translating coordinate system, in the (r, λ) directions. The azimuth λ is measured counterclockwise from the east. The constant Coriolis parameter f is evaluated at 20°N . The constant coefficient of eddy diffusion is K , and

$$\nabla^2 = \frac{1}{r} \frac{\partial}{\partial r} \left(r \frac{\partial}{\partial r} \right) + \frac{1}{r^2} \frac{\partial^2}{\partial \lambda^2} \quad (2)$$

is the horizontal Laplacian operation. Vertical advection of momentum into the boundary layer is small relative to horizontal advection, and is neglected.

The frictional drag F is quadratic and parallel to the total wind $\mathbf{u} + \mathbf{c}$ relative to the earth, i.e.,

$$F(\mathbf{c}, \mathbf{u}) = \frac{C_D}{h} |\mathbf{u} + \mathbf{c}| (\mathbf{u} + \mathbf{c}). \quad (3)$$

The drag coefficient C_D is assumed linear,

$$C_D = (\alpha + \beta |\mathbf{u} + \mathbf{c}|) \times 10^{-3}, \quad (4)$$

where the wind speed is in m s^{-1} . The linear relation used is that of Deacon (Roll, 1965), where $\alpha = 1.1$ and $\beta = 0.04$. The results of this study are not very sensitive to the choice of α and β within observational tolerances. The boundary layer depth h is assumed constant. This assumption, as well as the use of a constant eddy diffusivity, are discussed later in this section in the context of the numerical solution for a stationary vortex.

The pressure distribution $\phi \equiv \phi_0(r)$ is assumed symmetric and in gradient balance with a specified vortex with gradient wind $v_{gr}(r)$, so that

$$\frac{\partial \phi_0}{\partial r} \equiv \frac{v_{gr}^2}{r} + f v_{gr}. \quad (5)$$

The dashed line in Fig. 4 shows the gradient wind profile v_{gr} that balances ϕ in (5). The maximum wind is 42 m s^{-1} at the radius $r_{\max} = 40 \text{ km}$. There is a cubic spline transition zone 30 km wide connecting the solid body rotation of the inner core to a $(r/r_{\max})^{-0.6}$ profile in the outer vortex, extending to $r = 1300 \text{ km}$.

Differences between the geostrophic steering current and the translation velocity, as well as variations

in the Coriolis parameter, will force asymmetries in the wind field (Willoughby, 1979), which are not included in the present analysis. When the hurricane vortex translates, the friction due to the translation velocity \mathbf{c} in (3) induces an asymmetric component to the flow. Asymmetric convergence, as noted in Section 2, modifies the distribution of convection and the structure of the hurricane. Nevertheless, the surface pressure field of a moving hurricane appears quite symmetric in comparison to the wind (cf. Hawkins and Imbembo, 1976; Hawkins and Rubsam, 1968). Observations in Hurricane Gert of 1982 indicate that the asymmetric part of the geopotential height had a typical maximum amplitude of 11 m near the RMW (Willoughby, personal communication, 1982). A scaling analysis indicates that the forcing near the RMW due to the asymmetry in geopotential may in fact be comparable to that due to asymmetric boundary layer friction. In any case, whatever the nature of the asymmetry in ϕ , the frictional response to a translating symmetric pressure field $\phi = \phi_0(r)$ will have a significant influence on the hurricane's distribution of boundary layer winds and convergence. The analysis of the effect of surface pressure asymmetries is beyond the scope of this present study.

In order to keep the analysis as simple as possible, a constant boundary layer depth $h = 1 \text{ km}$ is used in this study, corresponding to the approximate depth of the mixed layer in the undisturbed tropical atmosphere. It is recognized that h may in fact vary strongly with radius near the core of the storm. Observations are not, however, sufficient to specify the variation of h with any degree of confidence. In fact, as the RMW is approached, the boundary layer itself becomes ill-defined, as the air is pulled up into the active convection. The boundary layer depth of $h = 1 \text{ km}$ is the same as that used by Ooyama (1969) and Chow (1971) in their numerical simulations. In the present study, an assumed depth of $h = 500 \text{ m}$ was found to lead to excessive radial velocities. Anthes (1971) found that the use of a vertically-averaged boundary layer model gave radial velocities a factor of 2 larger than those obtained in a multi-level model. For the present analysis the complications of either a multi-level model or a radially varying layer depth are considered beyond the level of sophistication required and knowledge of physics available. The essential conclusions of the present analysis concerning the dependence of winds and convergence distribution on the translation speed of the hurricane would not be expected to be altered by a more sophisticated boundary layer physics.

If the hurricane is stationary, $\mathbf{c} = 0$ so that the symmetric pressure field drives a symmetric boundary layer wind $\mathbf{u}_0(r)$, with $\partial/\partial\lambda = 0$ in (1). The momentum equations are solved by integration of (1), including time-derivative terms ($\partial\mathbf{u}/\partial t$, not shown) to

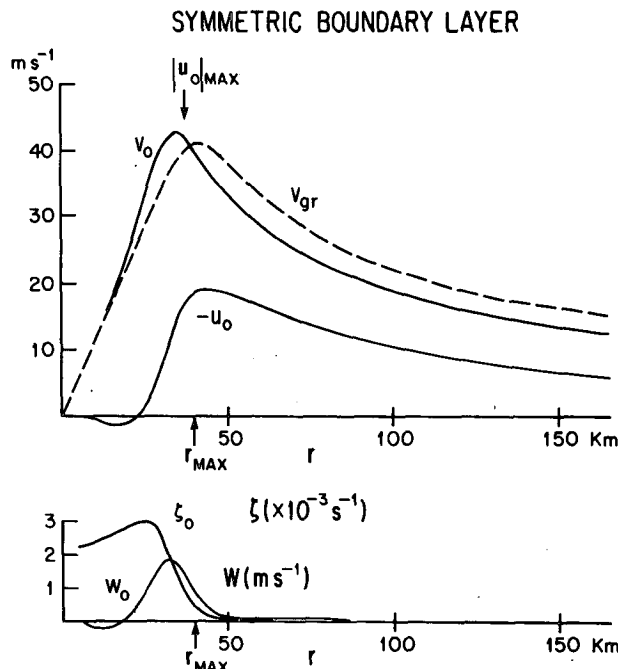


FIG. 4. Symmetric boundary response to stationary gradient vortex. Upper graph shows gradient wind (dashed line), and boundary layer wind \mathbf{u}_0 (solid lines). Lower graph shows boundary layer vorticity ζ_0 and vertical velocity w_0 at top of boundary layer.

a steady state for a specified $\phi(r)$. A Matsuno two-step time integration is used. This method (Matsuno, 1966) is second order, with no computational mode. It has the advantage that the steady-state solution is neutral. Since the method damps high-frequency oscillations in time, instability is manifested by steady small-scale spatial oscillations (cf., Anthes, 1971). A time step of 50 s is used. The grid spacing is variable, with uniform grid interval $\Delta r = 5$ km in $0 < r \leq 2r_{\max}$. In $r > 2r_{\max}$, the spacing increases linearly with radius, with the domain extending to $r = 1300$ km. The vorticity, $\zeta_0 = r^{-1}\partial(rv_0)/\partial r$, and vertical velocity at the top of the boundary layer, $w_0 = -hr^{-1}\partial(ru_0)/\partial r$, are specified to equal zero at the outer boundary; the symmetric wind $u_0 = 0$ at $r = 0$. The minimum grid spacing $\Delta r = 5$ km $\gg h$ so that the assumption that the slab boundary layer is much thinner than the horizontal scale of motion is valid. Also, Δr is small enough to resolve the transition region between the inner and outer domains of the vortex near r_{\max} . A nearly steady state for u_0 is achieved from an initial gradient vortex in less than one simulated day.

The steady-state symmetric boundary layer response using $K = 5 \times 10^4 \text{ m}^2 \text{ s}^{-1}$ is shown in Fig. 4. Similar solutions have been derived by Anthes (1971) and others. Anthes (1971) also summarized some previous analyses. The wind is supergradient in $r < r_{\max}$ due to the inward radial advection of momentum inside the inertially stable core. The inertial "wall," evidenced by the rapid increase in vorticity (ζ_0) just inside r_{\max} , leads to the rapid deceleration of u_0 and strong boundary layer convergence. The maximum inflow is $-u_0 \approx 20 \text{ m s}^{-1}$ and the maximum vertical velocity $w_0 \approx 2 \text{ m s}^{-1}$. The RMW, designated by $|u_0|_{\max}$ in Fig. 4, has been moved slightly inward by the penetration of u_0 into $r < r_{\max}$ and by the resulting supergradient wind.

The radial scale of the variation of u_0 near r_{\max} , where radial gradients are large, is determined by a balance between radial advection $\partial(\frac{1}{2}u_0^2)/\partial r$ and diffusion $K\partial^2 u_0/\partial r^2$. Thus, the scale of variation is $\delta r \approx 2 \times (5 \times 10^4 \text{ m}^2 \text{ s}^{-1})/20 \text{ m s}^{-1} = 5$ km, which is compatible with the grid spacing $\Delta r = 5$ km. Use of K one-half as large (not shown) leads to a scale of variation too short to be resolved by the grid spacing. In practice, small-scale spatial oscillations then develop in the solutions. The use of a variable, deformation-dependent K does not change the results substantially and only adds unnecessary complexity. Anthes (1971), using $\Delta r = 10$ km, took values of K ranging from 5 to $25 \times 10^4 \text{ m}^2 \text{ s}^{-1}$, choosing the latter as most realistic. This value is much greater than that used in the present study.

4. Translating hurricane: Formulation

The relative wind is decomposed in a spectral representation,

$$\mathbf{u} = \mathbf{u}_0(r) + \mathbf{u}_1(r, \lambda) + \mathbf{u}_2(r, \lambda), \quad (6)$$

where the subscripts denote wavenumbers $n = 0, 1$ and 2. As in the previous section, the velocity vector \mathbf{u} represents the (radial, tangential) components of the wind. The truncation of the series at $n = 2$ is valid if the hurricane is not translating too rapidly, so that the major part of the asymmetric flow is confined to low wavenumbers. This approximation will be justified *a posteriori* in Section 5.

The solution for the symmetric part of the wind (u_0) was shown in Fig. 4 for a stationary hurricane. Asymmetries modify this component of the flow for a moving hurricane. The wavenumber $n = 1$ component of the wind is represented as

$$u_1 = U_{s1}(r) \sin \lambda + U_{c1}(r) \cos \lambda, \quad (7a)$$

including both a radial and azimuthal dependence. Similarly,

$$u_2 = U_{s2}(r) \sin 2\lambda + U_{c2}(r) \cos 2\lambda \quad (7b)$$

is the wavenumber 2 component. In what follows the hurricane translates to the north, so that

$$\mathbf{c} = (c \sin \lambda, c \cos \lambda). \quad (7c)$$

The direction of motion is arbitrary since an f -plane is used. Eqs. (6) and (7) are substituted into (1) to derive a set of momentum equations governing each wavenumber. The radial and tangential equations governing $n = 0$ are

$$u_0 \frac{\partial u_0}{\partial r} - \left(\frac{v_0^2}{r} + f v_0 \right) - \frac{\partial \phi}{\partial r} - K \left(\nabla^2 u_0 - \frac{u_0}{r^2} \right) + N(u_0) + F(\mathbf{c}, u_0) = 0, \quad (8a)$$

$$(\zeta_0 + f)u_0 - K \left(\nabla^2 v_0 - \frac{v_0}{r^2} \right) + N(v_0) + F(\mathbf{c}, v_0) = 0. \quad (8b)$$

The equations governing wavenumbers $n = 1$ and 2 are

$$u_0 \frac{\partial u_n}{\partial r} + \frac{\partial u_0}{\partial r} u_n - \left(\frac{2v_0}{r} + f \right) v_n + \frac{v_0}{r} \frac{\partial u_n}{\partial \lambda} - K \left(\nabla^2 u_n - \frac{u_n}{r^2} - \frac{2}{r^2} \frac{\partial v_n}{\partial \lambda} \right) + N(u_n) + F(\mathbf{c}, u_n) = 0, \quad (9a)$$

$$u_0 \left(\frac{\partial v_n}{\partial r} + \frac{v_n}{r} \right) + u_n (\zeta_0 + f) + \frac{v_0}{r} \frac{\partial v_n}{\partial \lambda} - K \left(\nabla^2 v_n - \frac{v_n}{r^2} + \frac{2}{r^2} \frac{\partial u_n}{\partial \lambda} \right) + N(v_n) + F(\mathbf{c}, v_n) = 0, \quad (9b)$$

where n may take either the value 1 or 2.

In (8) and (9), contributions to advection from in-

interactions with the symmetric component \mathbf{u}_0 are explicitly included. Nonlinear advective interactions between wavenumbers 1 and 2 that contribute to the given component are denoted N . For example, $N(u_0)$ includes contributions to $[u(\partial u/\partial r) - v^2 r^{-1} + v r^{-1}(\partial u/\partial \lambda)]$ from interactions between wavenumber $n = 1$ and itself (1×1) and $n = 2$ and itself (2×2). By convention, this is denoted $N(u_0) = N(u_0; 11, 22)$. Also, $N(v_0) = N(v_0; 11, 22)$. Similarly, for the other components, $N(u_1) = N(u_1; 12)$ and $N(u_2) = N(u_2; 11)$. These terms are presented explicitly in Eqs. (B1)–(B3) of Appendix B.

Frictional drag terms that contribute to the individual components are denoted in a similar manner. The contributions of wavenumbers 0 and 1 triple interactions to $n = 0$ are denoted $F(c, \mathbf{u}_0) = F(c, \mathbf{u}_0; 000, 011)$. Similarly, $F(c, \mathbf{u}_1) = F(c, \mathbf{u}_1; 001, 111)$ and $F(c, \mathbf{u}_2) = F(c, \mathbf{u}_2; 011)$. These terms are derived in Appendix B and are given in Eqs. (B11)–(B13).

Contributions to $N(\mathbf{u})$ from wavenumbers > 2 , and contributions to $F(c, \mathbf{u})$ from wavenumbers > 1 have been neglected. When the hurricane is stationary ($c = 0$), $\mathbf{u}_1 = \mathbf{u}_2 = 0$. When the hurricane is translating, \mathbf{u}_1 is directly forced by $F(c, \mathbf{u}_1)$ [cf., Eq. (B12)]. Then \mathbf{u}_0 , \mathbf{u}_1 and \mathbf{u}_2 are modified by asymmetric nonlinear interactions. In the following section, the potential error due to the neglect of higher order modes in $F(c, \mathbf{u})$ and $N(\mathbf{u})$ will be evaluated from the solution itself. In practice, the formulation is accurate to within about 25% for a hurricane with maximum gradient wind of 42 m s^{-1} and $c = 10 \text{ m s}^{-1}$.

The system of equations (8) and (9) is solved for \mathbf{u} by integration to a steady state, as in the case of the stationary vortex presented in Section 3. Since the radial dependence of both the sine and cosine parts of the $n = 1$ and $n = 2$ components must be evaluated, a system of 10 equations is actually solved. The boundary conditions on \mathbf{u}_0 are as in Section 3. At the outer boundary, the asymmetric part of the solution matches the environment, $-fv_n + F(u_n) = 0$ and $fu_n + F(v_n) = 0$. At $r = 0$, $\mathbf{u}_2 = 0$, and \mathbf{u}_1 is extrapolated from the interior with $\mathbf{u}_1(r = 0) = 2\mathbf{u}_1(r = \Delta r) - \mathbf{u}_1(r = 2\Delta r)$. The initial condition used is the symmetric solution for the stationary hurricane vortex shown in Fig. 4. The winds \mathbf{u}_1 and \mathbf{u}_2 are initially zero. It was necessary to average radially the last term in the expression in parentheses after K in (9) for numerical stability. Otherwise, the numerical method is exactly as in Section 3.

5. Translating hurricane: Evaluation of boundary layer flow

Using the method described in the previous section, the boundary layer flow is evaluated for the hurricane vortex translating at $c = 10 \text{ m s}^{-1}$. Fig. 5 shows the solution, including all wavenumbers through $n = 2$ and all the nonlinear interactions specified in

Section 4. The arrow in each panel points to the north, the direction of motion. A circle has been drawn at radius $r_{\max} = 40 \text{ km}$ from the center of the vortex. In Fig. 5a the radial wind relative to the translating vortex shows maximum inflow in the right-front quadrant for $r < r_{\max}$. At large radius the wind is from the east (right). As the air moves toward the center of the vortex it spirals cyclonically, and the maximum inflow rotates counterclockwise. The position of maximum inflow is consistent with the observations of Hughes (1952). Positive values of u in the left rear imply overshooting of air, as can be seen in the streamlines of Fig. 5b. As discussed in Section 6, the overall character of the wind distribution is not substantially changed when $c = 5 \text{ m s}^{-1}$. Thus, a comparison can be made between Figs. 5b and 5c, and the distribution of winds in Hurricane Frederic, which was translating at $\sim 5 \text{ m s}^{-1}$. The isotachs in Fig. 5b show a pattern very similar to both those observed in Hurricane Frederic (Fig. 1) and those calculated by Chow (1971). Winds on the left are stronger than those on the right. The isotach maximum, however, is ahead of the vortex, with maximum wind of 60 m s^{-1} at $r \approx 23 \text{ km}$. Due to the added translation velocity of the vortex, the winds relative to the earth, shown in Fig. 5c, are stronger on the right than on the left. Once again the pattern is very similar to that in Hurricane Frederic (Fig. 9 of Powell, 1982). Near $r = r_{\max}$, the inflow angle (not shown) is maximum in the right-front quadrant. For $r \geq 100 \text{ km}$, the maximum inflow angle is in the right rear, agreeing with Powell's (1982, his Fig. 6) analysis of Frederic.

Convergence, shown in Fig. 5d, has a distribution very similar to the result of Chow (1971). Maximum convergence extends from ahead of the vortex center into the right-front and right-rear quadrants. The maximum value of $40 \times 10^{-4} \text{ s}^{-1}$ corresponds to $w = 4 \text{ m s}^{-1}$ at the top of the boundary layer. A region of weak divergence occurs to the south of the center, implying an elongated hurricane eye.

The solutions shown in Fig. 5 are for $c = 10 \text{ m s}^{-1}$, about the same as Hurricane Allen's speed of motion. The comparison between convergence in Fig. 5d and radar reflectivity in Fig. 3 is quite good, including the concentration of convergence and convection in the front to right-front quadrant [30 dB(Z), above] and the elongated clear eye. Although the overall character of the wind distribution is not substantially changed when $c = 5 \text{ m s}^{-1}$, the wind gradients, and thus the patterns of convergence, do change significantly. The characteristics of the convective distribution in Hurricane Frederic (Fig. 2) compare most favorably with the quasi-linear solution in Section 6, valid for a slowly moving vortex.

For a stronger, tighter vortex with $v_{gr} = 60 \text{ m s}^{-1}$ at $r_{\max} = 20 \text{ km}$, the solutions (not shown) have isotach and convergence distributions in $r < r_{\max}$ very

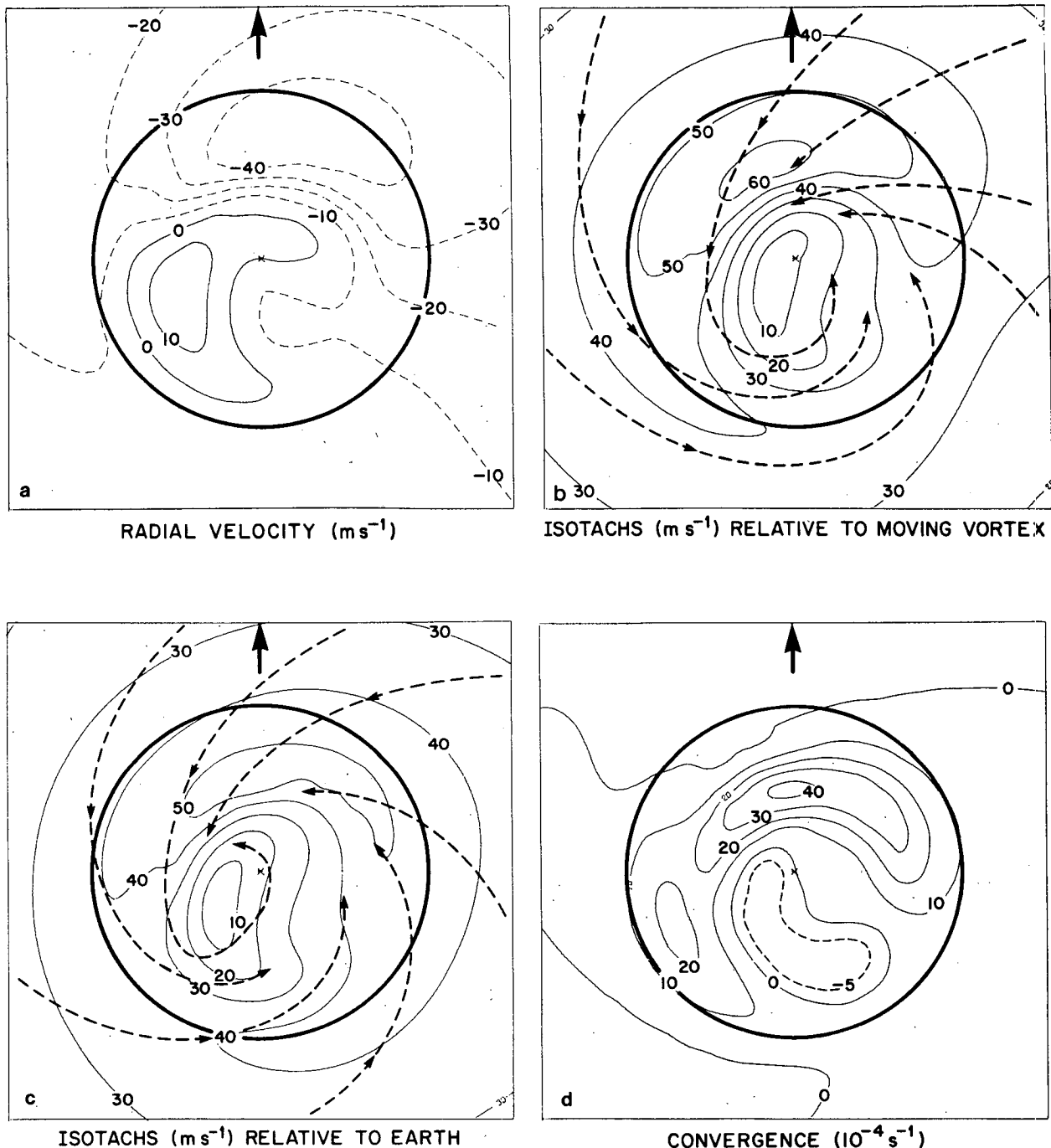


FIG. 5. (a) Radial velocity in complete (nonlinear) solution relative to translating vortex. Vortex is moving in direction of arrow at 10 m s^{-1} . Circle is at 40 km radius from center of vortex. (b) As in Fig. 5a, but for isotachs relative to translating vortex. Dashed lines are streamlines. (c) As in Fig. 5a, but for isotachs relative to earth. (d) As in Fig. 5a, but for convergence.

similar to those in Fig. 5. The strength of the wind asymmetry is greater than that in Figs. 5a and b by $\sim 50\%$, in proportion to the strength of the vortex. Due to the greater wind asymmetry, winds on the left are greater than those on the right relative to the earth, in contrast with Fig. 5c. The distribution of conver-

gence is very much the same as that in Fig. 5d, with the strength of the asymmetry about doubled.

In the formulation of Section 4 and Appendix B several approximations were made that can be tested *a posteriori* from the solution. Table 1 shows the maximum amplitude of each wavenumber compo-

TABLE 1. Maximum amplitude (m s^{-1}) of wavenumber 0, 1, and 2 components of solution. Translation speed $c = 10 \text{ m s}^{-1}$.

	Nonlinear	Linear friction	Linear	Quasi-linear
u_0	21	19	19	19
u_1	27	22	32	22
u_2	14	11		10
v_0	36	38	43	43
v_1	19	15	20	15
v_2	9	7		7

nent, occurring near the RMW. The first column refers to the nonlinear¹ solution given in Fig. 5. Since the magnitude of $u_1 = 27 \text{ m s}^{-1}$ is greater than $u_0 = 21 \text{ m s}^{-1}$, the asymmetric part of the solution in the boundary layer cannot be considered a small disturbance on the symmetric vortex. Since $u_2/u_1 \approx 1/2$, the $n = 2$ contribution is relatively small, however. In effect, the wavenumber $n = 0$ and $n = 1$ solutions together comprise the "basic state," to which an $n = 2$ "perturbation" is added. The $n = 1$ contribution is directly forced by the motion, adding to the symmetric component; the $n = 2$ contribution is forced indirectly through interaction among the lower-wavenumber components. Since $n = 3$ is forced by advective interaction between $n = 1$ and $n = 2$, we can estimate $u_3/u_2 \approx (u_1 \times u_2)/(u_1 \times u_1) \approx u_2/u_1 \approx 1/2$. Thus, $u_3/u_1 \approx 1/4$, so that wavenumber 3 (and higher) contributions to the solution may be neglected up to an error of $\sim 25\%$. At larger radius, u_2/u_1 is smaller so that the error is less. This degree of approximation is consistent with the neglect of terms in the expansion of the frictional drag given in Appendix B.

Similarly, the neglect of $n > 1$ in the frictional drag can be evaluated. The frictional drag $F(\mathbf{u}) \sim G\mathbf{u}$, where G is a drag coefficient associated with \mathbf{u} , analogous to $C_D|\mathbf{u}|/h$; G is defined explicitly after (B13a) in Appendix B. At large radius, $u_2/u_1 \ll 1$, so that $F(\mathbf{u}_2)/F(\mathbf{u}_1) \approx Gu_2/Gu_1 \ll 1$. Near the RMW, $u_2/u_1 \leq 1/2$. Then, $Gu_2/(v_0 u_1/r) \leq 1/4$ by direct analysis of the solution. Thus, the contribution of the $n = 2$ frictional forcing to the momentum balance is small relative to either the $n = 1$ frictional or advective contribution. Once again the potential error $\leq 25\%$.

Recently, Vic Ooyama of NHRL (personal communication, 1982) has made a numerical simulation of the boundary layer response under a translating vortex, using a spline method on a multi-nested Cartesian grid. The simulation was made as a developmental test of the numerical model, which will later be applied to more general forecast problems. The

specification of the physical parameters is identical to that in the present analysis. The spline results include, implicitly, azimuthal wavenumber interactions of much higher order than those contained in the present truncated spectral formulation. Nevertheless, a direct comparison of the solutions indicates that the distribution of convergence is very much the same in both formulations, except that in Ooyama's result the magnitude is reduced overall by $\sim 5 \times 10^{-4} \text{ s}^{-1}$ relative to that shown in Fig. 5d, and the pattern is rotated clockwise by $\sim 20^\circ$. The good agreement between the solutions confirms that the truncated spectral formulation approximates the fully nonlinear solution (including all wavenumbers) to within better than 25%. In Section 7 the role of asymmetric advective nonlinearities in limiting the amplitude of the response and rotating the distribution of convergence clockwise is described. The presence of stronger nonlinear interactions in Ooyama's simulation is consistent with this discussion. The qualitative results shown in this paper do not depend on the nonlinear interactions omitted in the present truncated spectral formulation.

6. Quasi-linear analysis

To simplify the analysis of the solution in Section 5, several *ad hoc* approximations will be made. First, in order to isolate the effect of asymmetric interactions on advection, the wave component interactions $0 \times 1 \times 1$ and $1 \times 1 \times 1$ will be suppressed in the frictional terms. Thus, $F(\mathbf{c}, \mathbf{u}_0) = F(\mathbf{c}, \mathbf{u}_0; 000)$, $F(\mathbf{c}, \mathbf{u}_1) = F(\mathbf{c}, \mathbf{u}_1; 001)$ and $F(\mathbf{c}, \mathbf{u}_2) = 0$. The qualitative behavior of the solution is changed very little by this simplification. In particular, the distribution of convergence (not shown) is very similar to that of Fig. 5d. The magnitudes of the asymmetric wave components, given in the second column of Table 1 as the "linear friction" solution, are reduced by $\sim 20\%$ due to the suppression of part of the frictional forcing.

Under the assumption that c , $|\mathbf{u}_1|$, $|\mathbf{u}_2| \ll |\mathbf{u}_0|$, a formulation completely linear in the asymmetries can be derived. In that case, $N(\mathbf{u}_0) = N(\mathbf{u}_1) = N(\mathbf{u}_2) = 0$ so that $|\mathbf{u}_1| \propto c$ and $\mathbf{u}_2 \equiv 0$. The linear solution does not correctly match the environmental wind since $c > |\mathbf{u}_0|$ for large r . The linear approximation is not accurate when $c = 10 \text{ m s}^{-1}$ since, as noted in Section 6, $u_1 > u_0$ near $r = r_{\text{max}}$. Nevertheless, a comparison of the linear and nonlinear solutions allows a direct evaluation of the effect of nonlinear asymmetric interactions, which are completely absent in the linear formulation. Moreover, for smaller translation velocities the linear approximation becomes more accurate. For $c = 5 \text{ m s}^{-1}$ nonlinear effects are very small.

The third column of Table 1 indicates that for $c = 10 \text{ m s}^{-1}$ the magnitude of the $n = 1$ component is greatly overestimated in the linear solution, with $|\mathbf{u}_1|$ (linear) $> |\mathbf{u}_1|$ (linear friction) by $\sim 40\%$. The mechanism by which the amplitude of \mathbf{u}_1 is limited

¹ Throughout this paper, "nonlinear" will denote interactions between asymmetric components. Interactions between the symmetric part of the flow and a single asymmetric component are "linear."

by nonlinear asymmetric advective interactions is discussed in Section 7. In order to visualize the entire linear solution, the magnitude of \mathbf{u}_1 will be artificially reduced by a factor of 1.4 so as to agree with the linear friction solution. Together, wavenumber $n = 0$ and $n = 1$ then comprise the basic state. The $n = 2$ perturbation is forced only by a wavenumber 1×1 interaction; this interaction is completely absent in the purely linear formulation. For the purpose of completeness, $N(\mathbf{u}_2; 11)$ will be retained, so that $\mathbf{u}_2 \neq 0$. Since $N(\mathbf{u}_0) = N(\mathbf{u}_1) = 0$ still, there is no feedback from higher wavenumbers to lower ones. The magnitude of the individual components in this quasi-linear solution are given in the last column of Table 1. It must be emphasized that the reduction of the amplitude of \mathbf{u}_1 and inclusion of $N(\mathbf{u}_2; 11)$ in the quasi-linear solution is *ad hoc*. The purpose is to isolate and visualize the effect of nonlinear asymmetric advective interactions on the $n = 0$ symmetric flow, and on the $n = 1$ asymmetric flow induced by the translation.

The quasi-linear solution is presented in Fig. 6. In common with the nonlinear solution in Section 5, maximum inflow (Fig. 6a) occurs in the right-front quadrant; outflow is evident in the left rear (cf. Fig. 5a). Winds relative to the translating vortex (Fig. 6b) are similarly stronger on the left than right, with major asymmetry front to back (cf. Fig. 5b). The RMW is at $r \approx 30$ km, farther out than in the nonlinear solution. Although the overall character of the wind distribution in the nonlinear solution is simulated in the quasi-linear context, differences are large enough that the pattern of convergence is significantly altered. The concentration of convergence in the right-front quadrant in $r < r_{\max}$ seen in Fig. 5d is replaced by a broad arc ahead, and slightly to the left, of the vortex center near $r = r_{\max}$ in Fig. 6c. The mechanism by which the RMW is moved radially inward and convergence maximum is rotated clockwise by asymmetric interactions is discussed in the following section.

As would be expected, fully nonlinear solutions for $c = 5 \text{ m s}^{-1}$ (not shown) closely resemble those in Fig. 6 since the nonlinear effects are then very small. The amplitude of the asymmetric part of the response is reduced, due to the slower storm translation speed. Hurricane Frederic was moving at $\sim 5 \text{ m s}^{-1}$. The distribution of high radar reflectivity in Fig. 2, with the broad arc of convection ahead of the hurricane and the nearly circular eye, compares favorably with convergence in Fig. 6c. Hurricane Floyd of 1981, which was also moving at $\sim 5 \text{ m s}^{-1}$, had a very similar reflectivity pattern, with the arc of high reflectivity oriented $\sim 30^\circ$ to the left of the direction of motion.

7. Diagnostic analysis

In a slowly moving hurricane, dissipation of vorticity in the boundary layer is balanced by production

of vorticity by convergence. Thus, there is a broad arc of convergence in front of the vortex in Fig. 6c. For a faster moving hurricane, advective effects modify the flow. Comparison of Figs. 5 and 6 indicates that faster translation of the hurricane tends to move the RMW radially inward, as well as to concentrate both gradients and convergence more toward the right side of the storm. In this section the role of advective nonlinearities in production of these tendencies, as well as in limitation of the amplitude of the asymmetries, will be analyzed.

Table 2 displays the dominant terms in the momentum balance for \mathbf{u}_1 in the linear and quasi-linear solutions of the previous section. The radial variation of \mathbf{u}_1 is determined by a balance among radial advection, centrifugal and Coriolis accelerations, tangential advection, diffusion, and forcing by frictional drag. At large radius ($r \gtrsim 200$ km) the balance is determined locally between frictional drag and tangential advection, and centrifugal and Coriolis accelerations. Radial advection imports momentum for $r \lesssim 100$ km, and dominates over frictional forcing in the u_1 budget for $r \lesssim 50$ km. For $r \lesssim r_{\max} = 40$ km the inertial acceleration $\zeta_0 u_1$ generated by the advection of u_1 into the highly stable core is balanced by tangential advection and diffusion of v_1 .

The amplitudes of the radial and tangential components of \mathbf{u}_1 in the linear solution are shown in Fig. 7. In the linear formulation $\mathbf{u}_0(r)$ is the same as the stationary solution in Fig. 4. At radii where $u_0(\partial \mathbf{u}_1 / \partial r)$ can be neglected, it can be shown that the phase angle where u_1 is a maximum is at azimuth $\lambda = \Theta(u_1)$, where

$$\Theta(u_1) = \tan^{-1} \frac{U_{s1}}{U_{c1}} \approx \text{Arctan} \left(\frac{G_0 + u_0 r^{-1}}{3v_0 r^{-1} + f} \right) + \pi, \quad (10a)$$

and that of v_1 is at

$$\Theta(v_1) \approx \text{Arctan} \left(\frac{G_0 + \partial u_0 / \partial r}{\zeta_0 + v_0 r^{-1} + f} \right) + \frac{\pi}{2}. \quad (10b)$$

Here $G_0 = (\alpha |\mathbf{u}_0| + \beta |\mathbf{u}_0|^2) h^{-1}$, a drag coefficient associated with the symmetric wind, analogous to $C_D |\mathbf{u}_0| h^{-1}$. G_0 is defined so that $F(\mathbf{c}, \mathbf{u}_1) \sim G_0(\mathbf{c} + \mathbf{u}_1)$. When $\Theta(u_1)$ and $\Theta(v_1)$ increase, the wind direction at a given azimuth tends to rotate counterclockwise.

Wind barbs depicting \mathbf{u}_1 in geographical coordinates are shown in Fig. 8 for $r = 25, 40, 100, 150$ and 500 km, at selected azimuths. At very large radius, $3v_0 r^{-1} + f \approx \zeta_0 + v_0 r^{-1} + f \approx f$, and $G_0, \partial u_0 / \partial r, u_0 / r \ll f$. The environmental flow is from the east with $\Theta(u_1) \approx \pi$ and $\Theta(v_1) \approx \pi/2$. Thus, at $r = 500$ km the wind blows nearly from the right (east) at any azimuth. As seen in Fig. 8, the direction of \mathbf{u}_1 varies to some extent with azimuth. At decreasing radius in $r > r_{\max}$, frictional drag (G_0) and $\partial u_0 / \partial r$ increase so that $\Theta(u_1)$ increases, rotating the wind direction at a given azimuth counterclockwise. The direction

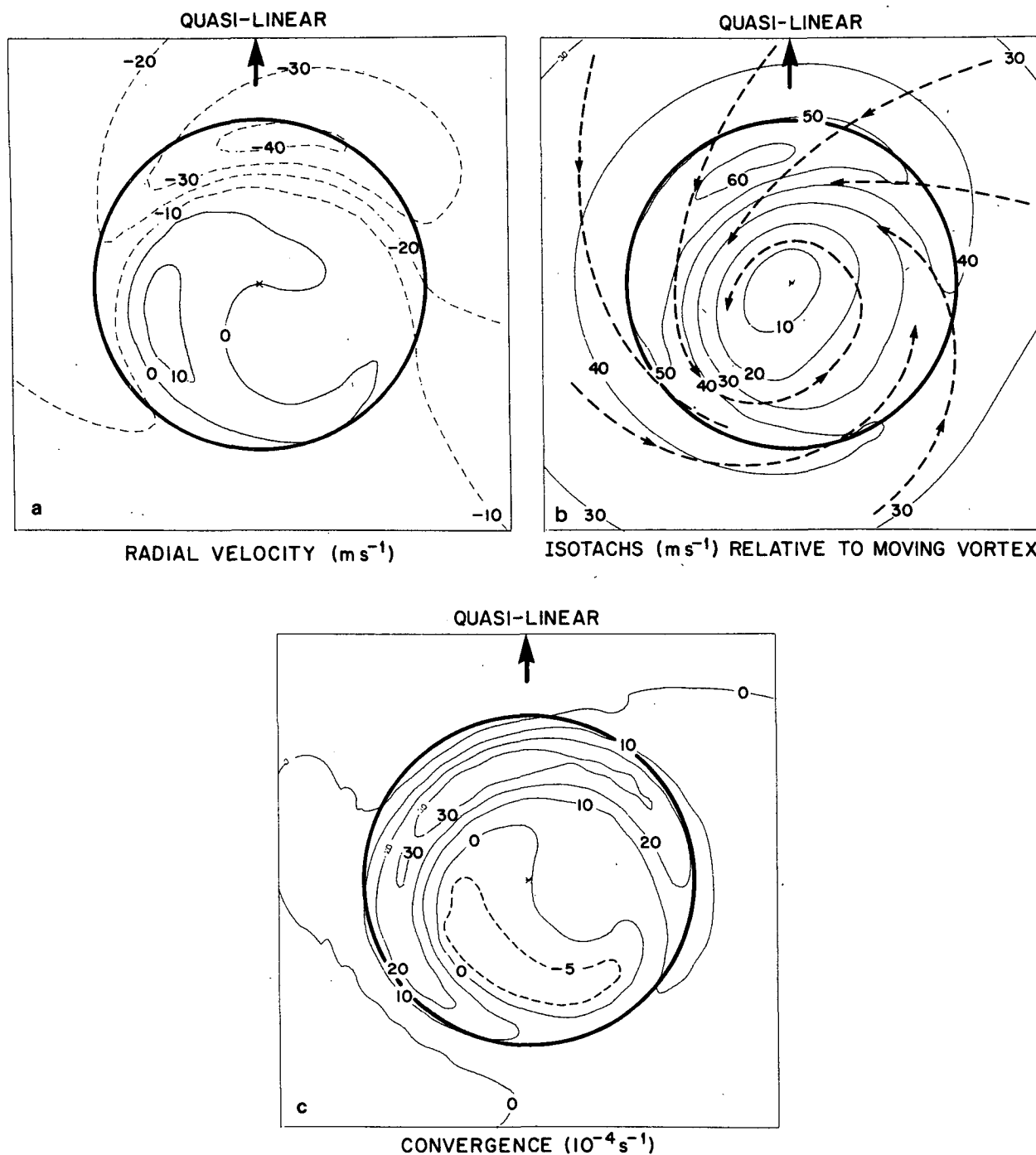


FIG. 6a-c. As in Figs. 5a, 5b and 5d, but for quasi-linear solution.

of \mathbf{u}_1 tends to rotate from east to north. On the left, \mathbf{u}_1 adds to the symmetric vortex circulation \mathbf{u}_0 , so that $|\mathbf{u}_0 + \mathbf{u}_1|$ is greater on the left than on the right relative to the moving vortex.

Near $r = r_{\max}$, the magnitude of $u_0(\partial u_1 / \partial r)$ becomes so large that (10a) and (10b) are no longer valid. The amplitude of u_1 is maximum in $r < r_{\max}$, where u_0

is rapidly decelerating ($\partial u_0 / \partial r \ll 0$); v_1 is maximum where u_0 itself approaches zero, at somewhat smaller radius. Since the maximum of $|\mathbf{u}_1|$ occurs in $r < r_{\max}$, the isotach maximum moves inward due to the storm translation. The RMW decreases from $r \approx 38$ km in the stationary hurricane (Fig. 4) to $r \approx 33$ km in the quasi-linear formulation (Fig. 6b). An independent

TABLE 2. Momentum budgets for u_1 and v_1 ; linear and quasi-linear solution. Dominant terms in the momentum equations are designated by one, two or three asterisks, in increasing order of their contribution to the balance.

Radius r (km)	$u_0 \frac{\partial u_1}{\partial r} + \frac{\partial u_0}{\partial r} u_1 - \left(\frac{2v_0}{r} + f \right) v_1 + \frac{v_0}{r} \frac{\partial u_1}{\partial \lambda} - K \nabla^2 u_1 + F(c, u_1)$				
500			***		***
200	*	**	***	**	**
100	**	**	***	***	**
50	**	*	***	***	
30	*	**	***	**	*
	$u_0 \left(\frac{\partial v_1}{\partial r} + \frac{v_1}{r} \right) + (\zeta_0 + f) u_1 + \frac{v_0}{r} \frac{\partial v_1}{\partial \lambda} - K \nabla^2 v_1 + F(c, v_1)$				
500			***		***
200			**	*	***
100		**	***	***	***
50		**	***	***	**
30			***	**	**

analysis (not shown) confirms the role of radial advection in reducing the RMW in the quasi-linear solutions; with $u_0 \equiv 0$, $|u_1|$ is maximum in $r > r_{\max}$.

Advection of u_1 by u_0 into the highly stable core in $r < r_{\max}$ has another effect on the position of the isotach maximum. In $r < r_{\max}$, ζ_0 increases rapidly (Fig. 4). Then, as implied by (10b), $\Theta(v_1)$ decreases rapidly inward [$\partial\Theta(v_1)/\partial r > 0$]. Thus at decreasing radius for $r < r_{\max}$, the direction of u_1 rotates clockwise, as seen in Fig. 8. The maximum of v_1 occurs in the left-front quadrant. The isotach maximum occurs more nearly in front of the storm (cf. Fig. 6b) due to the additional contribution of u_1 . In the absence of radial advection of momentum into $r < r_{\max}$, the isotach maximum would shift in the counter-clockwise direction.

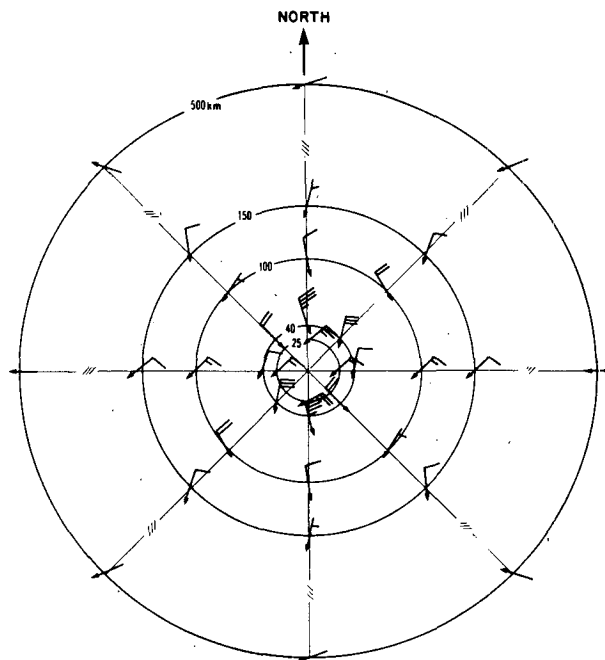


FIG. 8. Wind barbs depicting linear response u_1 in geographical coordinates for $r = 25, 40, 100, 150$ and 500 km at selected azimuths. A full barb represents 5 m s^{-1} , a half barb 2.5 m s^{-1} . The direction of storm translation is toward the top of figure.

Quasi-linear effects explain the wind and convergence distribution for a hurricane vortex translating at $c \approx 5 \text{ m s}^{-1}$. Differences between Figs. 5 and 6 must be understood, however, in terms of the contribution of nonlinear advective interactions for a hurricane moving at $c = 10 \text{ m s}^{-1}$. Two sets of terms in the momentum equations, $N(u_0; 11, 22)$ and $N(u_1; 12)$, representing the feedback of $n = 1$ and $n = 2$

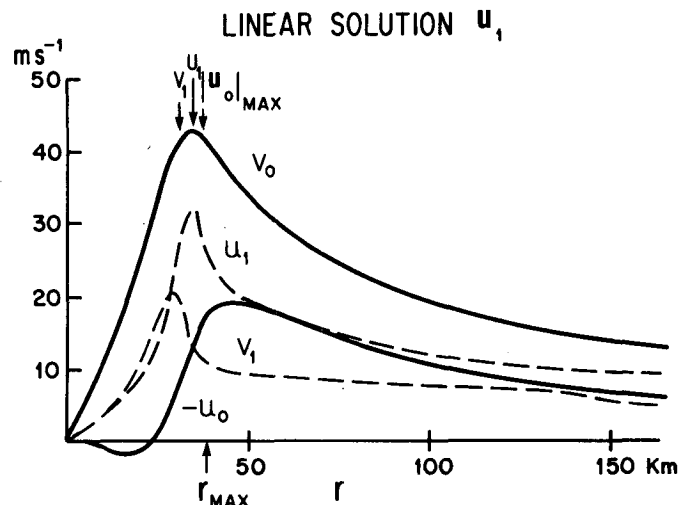


FIG. 7. Linear boundary layer response to translating vortex. Solid lines are symmetric winds u_0 , as in Fig. 4. Dashed lines are amplitudes of components of linear response u_1 .

interactions to the structure of lower-order modes, account for the differences. The contribution of each of the two sets will be considered separately below.

Fig. 9 shows the solution for u_0 , both with and without the $N(u_0; 11, 22)$ contribution included. The latter case corresponds to the quasi-linear formulation; the former includes modification of the symmetric component by rectification of the $n = 1$ (and, to a much lesser extent, $n = 2$) asymmetry.

The largest values of $N(u_0)$ appear in $N(v_0)$ near the very sharp gradient of v_1 in Fig. 7 at $r \approx 35$ km. The dominant contribution to $N(v_0)$ is

$$\frac{1}{2\pi} \int_0^{2\pi} u_1 \frac{\partial v_1}{\partial r} d\lambda.$$

With u_1 nearly from the north, it is easy to show that $N^0(v_0) \propto \partial\Theta(v_1)/\partial r > 0$, as noted above. $N(v_0) > 0$ acts as a drag term, reducing the amplitude of the peak in v_0 , as can be seen in Fig. 9. The sharpness of the ζ_0 inertial wall in $r < r_{\max}$ is thereby reduced, allowing u_0 to penetrate further inward. Thus the deceleration of u_0 , $(\partial u_0/\partial r)/u_0$, is significantly reduced near r_{\max} .

The modification of u_0 by $N(u_0; 11, 22)$ described above also affects u_1 , as shown in Fig. 10. The reduced deceleration of u_0 in $r < r_{\max}$ reduces the acceleration of u_1 . This is the mechanism by which the asymmetric nonlinear interactions limit the amplitude of u_1 . Since u_0 penetrates further into $r < r_{\max}$ (Fig. 9),

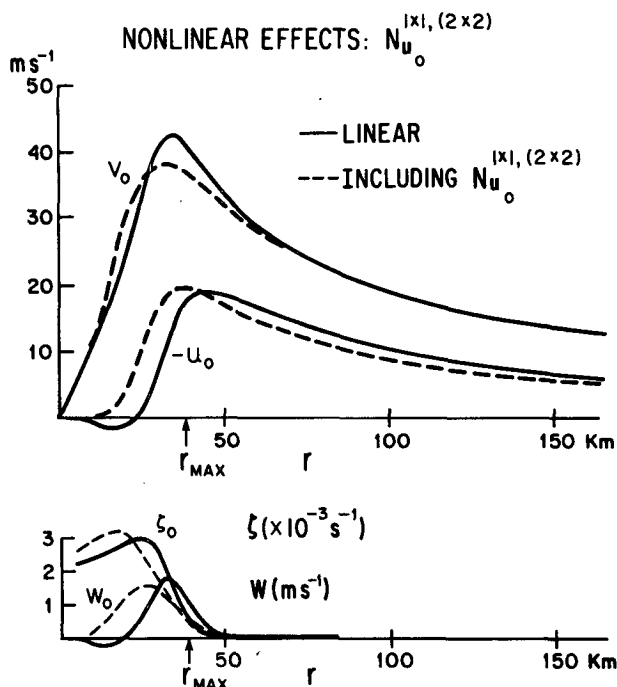


FIG. 9. Effect of asymmetric nonlinear interactions $N(u_0; 11, 22)$ on symmetric boundary layer response. Solid lines are without nonlinear interactions, as in Fig. 4. Dashed lines include nonlinear advective terms.

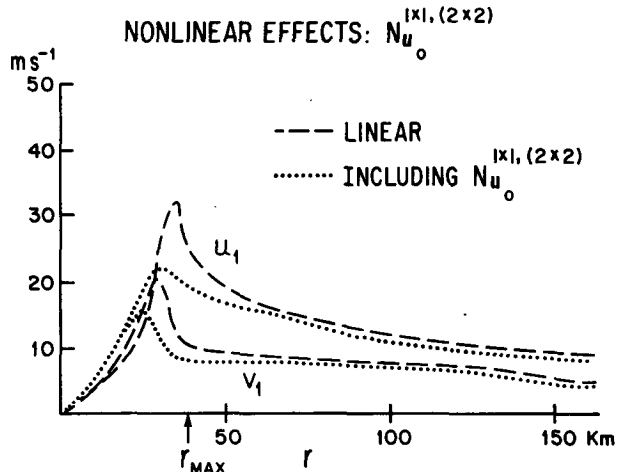


FIG. 10. Effect of asymmetric nonlinear interactions on asymmetric boundary layer response. Dashed lines are linear response u_1 , as in Fig. 7. Dotted lines are response including nonlinear advective terms.

the maximum of $|u_1|$ also occurs further inward. Thus, nonlinear interactions tend to move the RMW inward of the quasi-linear solution. The net effect of the translation of the vortex at 10 m s^{-1} is to move the RMW inward from $r \approx 38$ km for the stationary vortex to $r \approx 28$ km. The additional frictional drag included in the nonlinear solution of Section 5 further reduces the RMW to $r \approx 23$ km.

The value of u_1 is modified by wavenumber 1×2 interactions as well, included in $N(u_1; 12)$. In $r \leq 100$ km, the direction of u_1 is such that v_1 advects air on the right side of the storm against the symmetric wind v_0 . Thus, a "weakness" is induced on the right side, allowing air parcels to move more directly into the center. This description is analogous to one given by Myers and Malkin (1961). Also, u_1 advects air inward, augmenting u_0 on the right side. Thus, the maxima of u and w are rotated clockwise, and also strengthened to the right of the direction of translation.

8. Summary and discussion

The diagnosed asymmetry in the boundary layer response is forced by the asymmetry in frictional drag, due to the translation of the storm. The substantial wind asymmetries near the storm center cannot, however, be evaluated as simply a local response to the drag. Radial advection plays an important role, importing momentum into the inner core. Influences outside the boundary layer also contribute to the asymmetry of a hurricane. Asymmetries in the large-scale environment, convective heat release and the structure of the winds above the boundary layer may play a role. The simple slab model with constant depth used in the present analysis cannot describe the detailed structure of the boundary layer, especially

near the convectively active eye wall. Nevertheless, the characteristics of the quasi-linear and nonlinear solutions in the present truncated spectral formulation would be expected to be significant in determining the asymmetric structure of a moving hurricane.

Detailed observations of asymmetries in the boundary layer of translating hurricanes are quite limited. Powell's analysis of Hurricane Frederic is probably the most complete. Radar observations of reflectivity, from which the convective structure can be deduced, are more readily available. Examples were given from Hurricanes Frederic and Allen in Section 2. Although considerable variability exists in the convective structure of these storms, general agreement is found between the observed spatial distributions of convection in the moving hurricanes and boundary layer convergence determined by the present simple boundary layer model.

For a relatively slowly moving hurricane ($c \leq 5 \text{ m s}^{-1}$) the linear/quasi-linear formulation of Section 6 is valid. Inflow is maximum in the right-front quadrant (Fig. 6a). Convergence (Fig. 6c) is large in a broad arc ahead of the center of the storm. Divergence occurs within a nearly circular eye. Winds relative to the moving vortex are stronger on the left than right (Fig. 6b). The maximum winds lie nearly ahead of the storm, due to the advection of momentum into the highly stable core (Section 6). The distribution of winds in Hurricane Frederic (Fig. 1; and Powell, 1982) as well as radar reflectivity (Fig. 2) agree qualitatively with these results.

When the translation speed is increased ($c \geq 10 \text{ m s}^{-1}$), nonlinear asymmetric advective interactions become stronger. As the solution of Section 5 shows, inflow (Fig. 5a) and convergence (Fig. 5d) become concentrated more ahead and to the right of the storm. The divergent eye becomes more elliptical. The radar reflectivity distribution in Hurricane Allen (Fig. 3), which was translating at about 10 m s^{-1} , shows evidence of these characteristics. Due to increased advection of momentum into the core, the RMW tends to contract. For the case shown in Fig. 5, the motion of the vortex decreased the RMW by $\sim 15 \text{ km}$. In the present analysis, however, the distribution of pressure is specified. The feedback of the modified distribution of convergence to the pressure field has not been included. If the pressure did adjust, the full predicted reduction of the RMW might not actually occur.

Although the truncated spectral formulation used in this paper includes only modes through wavenumber 2, the *a posteriori* analysis in Section 5 indicates that it approximates the fully nonlinear solution (including all wavenumbers) to within $\sim 25\%$. The solution in Fig. 5 agrees overall with the fully nonlinear simulation of Chow (1971), and with Ooyama's recent calculations.

An obvious extension of the present analysis would

be a study of the time evolution of the boundary layer under a turning vortex. Here a fully nonlinear rather than a spectral model would be appropriate. Comparison with observations would be even more difficult than in the present analysis, since composites would not be as useful.

Acknowledgments. I would like to acknowledge with thanks many valuable discussions with Vic Ooyama during the course of this study, as well as his comments on earlier versions of this paper. Discussions with Hugh Willoughby have also been very constructive. His comments on the manuscript, as well as those of Steve Lord and Kim Paradis, have helped me considerably. I thank Dave Jorgensen and Frank Marks for the radar composites, and Mark Powell for the Frederic data. Dale Martin drew the figures; the high quality of his work speaks for itself. Angel Tillman's expert typing skills, especially with the equations, made preparation of this paper so much easier.

APPENDIX A

List of Symbols

r	radius
λ	azimuth, measured counterclockwise from east
$\mathbf{U} = (u, v)$	(radial, tangential) velocity relative to translating coordinate system
n	azimuthal wavenumber
u_n	spectral components of horizontal velocity (wavenumber $n = 0, 1, 2$)
$U_{sn}(r),$ $U_{cn}(r)$	radial variation of sine (s) or cosine (c) component of (radial, tangential) velocity (wavenumber $n = 1, 2$)
f	Coriolis parameter
ϕ	specified symmetric geopotential [$=\phi_0(r)$]
K	eddy diffusion
c	translation velocity of vortex
$F(c, \mathbf{u})$	boundary layer frictional drag on \mathbf{u}
C_D	drag coefficient
α, β	coefficients in linear drag law
h	boundary layer depth
v_{gr}	gradient wind
r_{max}	radius of maximum gradient wind
Δr	grid spacing
ζ_0	vorticity of symmetric wind
w	vertical velocity at top of boundary layer
δr	radial scale of response
$N(\mathbf{u})$	contribution of asymmetric nonlinear advective terms to \mathbf{u} momentum balance
$\Theta(\mathbf{u}_i)$	phase angle of maximum u_i or v_i
G, H	drag coefficients associated with \mathbf{u} (defined in Appendix B)
G_0	drag coefficient associated with \mathbf{u}_0
$F(c, \mathbf{u}_n; ijk)$	contribution of wavenumber $i \times j \times k$ interactions to frictional drag on \mathbf{u}_n

$N(u_n; ij)$ contribution of wavenumber $i \times j$ interactions to asymmetric nonlinear advective terms in u_n momentum balance.

APPENDIX B

Derivation of Advective and Frictional Terms in Momentum Equations

Eq. (8a) in Section 4 is derived by substituting (6) and (7) into (1a) and collecting terms contributing to $n = 0$. The contribution to advection, $[u(\partial u/\partial r) - v^2 r^{-1} + vr^{-1}(\partial u/\partial \lambda)]$, by interaction between asymmetric components is $N(u_0)$. It is straightforward to derive

$$\begin{aligned} N(u_0) &= N(u_0; 11, 22) \\ &= (U_{s1}U'_{s1} + U_{c1}U'_{c1} + U_{s2}U'_{s2} + U_{c2}U'_{c2})/2 \\ &\quad - (V_{s1}^2 + V_{c1}^2 + V_{s2}^2 + V_{c2}^2)/2r + (-U_{c1}V_{s1} \\ &\quad + V_{c1}U_{s1} - 2U_{c2}V_{s2} + 2V_{c2}U_{s2})/2r, \quad (B1a) \end{aligned}$$

where a prime denotes differentiation with respect to r . When terms contributing to $n = 0$ in (1b) are collected, Eq. (8b) follows. The contribution to advection, $\{u[(\partial v/\partial r) + vr^{-1}] + vr^{-1}(\partial v/\partial \lambda)\}$, by asymmetric component interactions is

$$\begin{aligned} N(v_0) &= N(v_0; 11, 22) \\ &= [U_{s1}(V'_{s1} + V_{s1}/r) + U_{c1}(V'_{c1} + V_{c1}/r) \\ &\quad + U_{s2}(V'_{s2} + V_{s2}/r) + U_{c2}(V'_{c2} + V_{c2}/r)]/2. \quad (B1b) \end{aligned}$$

Similarly, for $n = 1$, Eqs. (9a) and (9b) follow with

$$\begin{aligned} N(u_1) &= N(u_1; 12) \\ &= [(U_{s2}U'_{c1} - U_{c2}U'_{s1} - U_{s1}U'_{c2} + U_{c1}U'_{s2})/2 \\ &\quad - (V_{s2}V_{c1} - V_{c2}V_{s1})/r + (-2V_{s1}U_{s2} \\ &\quad - 2V_{c1}U_{c2} + V_{s2}U_{s1} + V_{c2}U_{c1})/2r] \\ &\quad \times \sin \lambda + [(U_{s2}U'_{s1} + U_{c2}U'_{c1} + U_{s1}U'_{s2} \\ &\quad + U_{c1}U'_{c2})/2 - (V_{s2}V_{s1} + V_{c2}V_{c1})/r \\ &\quad + (-2V_{s1}U_{c2} + 2V_{c1}U_{s2} \\ &\quad - V_{s2}U_{c1} + V_{c2}U_{s1})/2r] \cos \lambda, \quad (B2a) \end{aligned}$$

$$\begin{aligned} N(v_1) &= N(v_1; 12) \\ &= [(U_{s2}\{V'_{c1} + V_{c1}/r\} - U_{c2}\{V'_{s1} + V_{s1}/r\} \\ &\quad - U_{s1}\{V'_{c2} + V_{c2}/r\} + U_{c1}\{V'_{s2} + V_{s2}/r\})/2 \\ &\quad + (-V_{s1}V_{s2} - V_{c1}V_{c2})/2r] \sin \lambda \\ &\quad + [(U_{s2}\{V'_{s1} + V_{s1}/r\} + U_{c2}\{V'_{c1} + V_{c1}/r\} \end{aligned}$$

$$\begin{aligned} &+ U_{s1}\{V'_{s2} + V_{s2}/r\} + U_{c1}\{V'_{c2} + V_{c2}/r\})/2 \\ &+ (V_{s2}V_{c1} - V_{s1}V_{c2})/2r] \cos \lambda. \quad (B2b) \end{aligned}$$

For $n = 2$,

$$\begin{aligned} N(u_2) &= N(u_2; 11) \\ &= [(U_{s1}U'_{c1} + U_{c1}U'_{s1})/2 - (V_{s1}V_{c1})/2r \\ &\quad + (V_{s1}U_{s1} - U_{c1}V_{c1})/2r] \sin 2\lambda \\ &\quad + [(-U_{s1}U'_{s1} + U_{c1}U'_{c1})/2 - (-V_{s1}^2 + V_{c1}^2)/2r \\ &\quad + (V_{s1}U_{c1} + V_{c1}U_{s1})/2r] \cos 2\lambda, \quad (B3a) \end{aligned}$$

$$\begin{aligned} N(v_2) &= N(v_2; 11) \\ &= [(U_{s1}\{V'_{c1} + V_{c1}/r\} + U_{c1}\{V'_{s1} + V_{s1}/r\})/2 \\ &\quad + (V_{s1}^2 - V_{c1}^2)/2r] \sin 2\lambda \\ &\quad + [(-U_{s1}\{V'_{s1} + V_{s1}/r\} \\ &\quad + U_{c1}\{V'_{c1} + V_{c1}/r\})/2 \\ &\quad + (V_{s1}V_{c1})/r] \cos 2\lambda. \quad (B3b) \end{aligned}$$

The derivation of the contribution of friction to (8) and (9) requires further analysis. From (3),

$$F(c, u) = C_D h^{-1} |u + c|(u + c \sin \lambda). \quad (B4)$$

Using (4),

$$F(c, u) = h^{-1} (\alpha |u + c| + \beta |u + c|^2) (u + c \sin \lambda), \quad (B5)$$

where

$$|u + c| = [(u + c \sin \lambda)^2 + (v + c \cos \lambda)^2]^{1/2}. \quad (B6)$$

After substituting from (6) and (7) for u and v in (B6), and assuming $u_2 = 0$, some algebra gives

$$|u + c| = [A + S]^{1/2}, \quad (B7)$$

where

$$\begin{aligned} S &= 2(E + B_s \sin \lambda + B_c \cos \lambda + C_s \\ &\quad \times \sin 2\lambda + C_c \cos 2\lambda), \quad (B8) \end{aligned}$$

and

$$\left. \begin{aligned} A &= u_0^2 + v_0^2 + (U_{s1}^2 + U_{c1}^2 + V_{s1}^2 + V_{c1}^2)/2 \\ &= \left(\int_0^{2\pi} |u|^2 d\lambda \right) / 2\pi \\ E &= (cU_{s1} + cV_{c1})/2 \\ B_s &= u_0 U_{s1} + v_0 V_{s1} + u_0 c \\ B_c &= u_0 U_{c1} + v_0 V_{c1} + v_0 c \\ C_s &= -(U_{s1}^2 + V_{s1}^2)/4 + (U_{c1}^2 + V_{c1}^2)/4 \\ &\quad - cU_{s1}/2 + cV_{c1}/2 \\ C_c &= (U_{s1}U_{c1} + V_{s1}V_{c1} + cU_{c1} + cV_{s1})/2 \end{aligned} \right\} \quad (B9)$$

The term $A > 0$, so (B7) can be expanded in a Taylor series,

$$(A + S)^{1/2} = A^{1/2} \left(1 + \frac{S}{2A} + \dots \right). \quad (\text{B10})$$

By inspection, $S/A \leq 3$ as a very conservative estimate. Then, retention of only the first two terms in the expansion (B10) results in an error of less than 25%. This degree of approximation is consistent with the other approximations in this analysis, as determined in Section 5. Thus, the evaluation of $|\mathbf{u} + \mathbf{c}|$ in (B5) includes only these two terms. Collecting terms that contribute to $n = 0$ gives, after some algebra,

$$\begin{aligned} F(\mathbf{c}, u_0) &= F(\mathbf{c}, u_0; 000, 011) \\ &= Gu_0 + HA^{-1}[(c + U_{s1})B_s/2 \\ &\quad + B_c U_{c1}/2 + u_0 E], \quad (\text{B11a}) \end{aligned}$$

where

$$\begin{aligned} G &\equiv h^{-1}(\alpha A^{1/2} + \beta A), \\ H &\equiv h^{-1}(\alpha A^{1/2} + 2\beta A). \end{aligned}$$

Here G is a drag coefficient analogous to $C_D|\mathbf{u} + \mathbf{c}|/h$, where $A^{1/2}$ takes the place of $|\mathbf{u} + \mathbf{c}|$. Since \mathbf{c} is a wavenumber 1 component, interactions between \mathbf{c} and other components are formally equivalent to interactions with \mathbf{u}_1 . Similarly,

$$\begin{aligned} F(\mathbf{c}, v_0) &= F(\mathbf{c}, v_0; 000, 011) \\ &= Gv_0 + HA^{-1}[V_{s1}B_s/2 \\ &\quad + (c + V_{c1})B_c/2 + v_0 E]. \quad (\text{B11b}) \end{aligned}$$

For $n = 1$,

$$\begin{aligned} F(\mathbf{c}, u_1) &= F(\mathbf{c}, u_1; 001, 111) \\ &= \{G(c + U_{s1}) \sin \lambda + GU_{c1} \cos \lambda + HA^{-1} \\ &\quad \times (u_0 B_s \sin \lambda + u_0 B_c \cos \lambda)\} + HA^{-1} \\ &\quad \times \{[-C_c(c + U_{s1})/2 + C_s U_{c1}/2 \\ &\quad + (c + U_{s1})E] \sin \lambda + [C_s(c + U_{s1})/2 \\ &\quad + C_c U_{c1}/2 + U_{c1}E] \cos \lambda\}, \quad (\text{B12a}) \end{aligned}$$

$$\begin{aligned} F(\mathbf{c}, v_1) &= F(\mathbf{c}, v_1; 001, 111), \\ &= \{GV_{s1} \sin \lambda + G(c + V_{c1}) \cos \lambda + HA^{-1} \\ &\quad \times (v_0 B_s \sin \lambda + v_0 B_c \cos \lambda)\} + HA^{-1} \\ &\quad \times \{[-C_c V_{s1}/2 + C_s(c + V_{c1})/2 + V_{s1}E] \\ &\quad \times \sin \lambda + [C_s V_{s1}/2 + C_c(c + V_{c1})/2 \\ &\quad + (c + V_{c1})E] \cos \lambda\}. \quad (\text{B12b}) \end{aligned}$$

For $n = 2$,

$$\begin{aligned} F(\mathbf{c}, u_2) &= F(\mathbf{c}, u_2; 011) \\ &= HA^{-1}\{[-B_s(c + U_{s1})/2 \\ &\quad + B_c U_{c1}/2 + C_c u_0] \cos 2\lambda + [B_s U_{c1}/2 \\ &\quad + B_c(c + U_{s1})/2 + C_s u_0] \sin 2\lambda\}, \quad (\text{B13a}) \end{aligned}$$

$$\begin{aligned} F(\mathbf{c}, v_2) &= F(\mathbf{c}, v_2; 011), \\ &= HA^{-1}\{[-B_s V_{s1}/2 - B_c(c + V_{c1})/2 + v_0 C_c] \\ &\quad \times \cos 2\lambda + [B_s(c + V_{c1})/2 \\ &\quad + B_c V_{s1}/2 + v_0 C_s] \sin 2\lambda\}. \quad (\text{B13b}) \end{aligned}$$

The neglect of wavenumber $n > 1$ is justified in Section 5.

The expressions for advection [(B1), (B2) and (B3)] and friction [(B11), (B12) and (B13)] enter the momentum equations (8) and (9) in Section 4.

REFERENCES

- Anthes, R. A., 1971: Iterative solutions to the steady-state axisymmetric boundary layer equations under an intense pressure gradient. *Mon. Wea. Rev.*, **99**, 261–268.
- Batchelor, G. K., 1967: *An Introduction to Fluid Dynamics*. Cambridge University Press, 615 pp.
- Chow, S., 1971: A study of the wind field in the planetary boundary layer of a moving tropical cyclone. M.S. thesis, Dept. Meteor. Oceanogr., New York University, 59 pp. [NOAA/NHRL Library, 1320 South Dixie Highway, Coral Gables, FL 33146.]
- Hawkins, H. F., and S. M. Imbembo, 1976: The structure of a small, intense Hurricane—Inez, 1966. *Mon. Wea. Rev.*, **104**, 418–442.
- , and D. J. Rubsam, 1968: Hurricane Hilda, 1964: II. Structure and budgets of the hurricane on October 1, 1964. *Mon. Wea. Rev.*, **96**, 617–636.
- Hughes, L. A., 1952: On the low-level wind structure of tropical storms. *J. Meteor.*, **9**, 422–428.
- Matsuno, J., 1966: Numerical integrations of the primitive equations by a simulated backward difference method. *J. Meteor. Soc. Japan*, **44**, 76–84.
- Myers, V. A., and W. Malkin, 1961: Some properties of hurricane wind fields as deduced from trajectories. NHRP Rep. 49, 45 pp. [NOAA/NHRL Library, 1320 South Dixie Highway, Coral Gables, FL 33146].
- Ooyama, K. V., 1969: Numerical simulation of the life-cycle of tropical cyclones. *J. Atmos. Sci.*, **26**, 3–40.
- , 1982: Conceptual evolution of the theory and modeling of the tropical cyclone. *J. Meteor. Soc. Japan*, **60**, 369–379.
- Powell, M. D., 1982: The transition of the Hurricane Frederic boundary-layer wind field from the open Gulf of Mexico to landfall. *Mon. Wea. Rev.*, **110**, 1912–1932.
- Roll, H. V., 1965: *Physics of the Marine Atmosphere*. Academic Press, 426 pp.
- Willoughby, H. E., 1979: Excitation of spiral bands in hurricanes by interaction between the symmetric mean vortex and a shearing environmental steering current. *J. Atmos. Sci.*, **36**, 1226–1233.
- , J. A. Clos and M. D. Shoreibah, 1982: Concentric eyewalls, secondary wind maxima, and the evolution of the hurricane vortex. *J. Atmos. Sci.*, **39**, 395–411.